Hindawi
Advances in Civil Engineering
Volume 2019, Article ID 4160804, 9 pages
https://doi.org/10.1155/2019/4160804

Research Article

Dynamic Mechanical Properties and Failure Mode of Artificial Frozen Silty Clay Subject to One-Dimensional Coupled Static and Dynamic Loads

Dong-dong Ma[1,2] **Qin-yong Ma**[1,2] **Zhao-ming Yao**[2] **Pu Yuan**[1,2] **and Rong-rong Zhang**[1,2]

[1]*Research Center of Mine Underground Engineering, Ministry of Education, Huainan, China*
[2]*Anhui University of Science and Technology, Huainan, Anhui 232001, China*

Correspondence should be addressed to Qin-yong Ma; qymaah@126.com

Received 18 August 2018; Revised 26 February 2019; Accepted 27 March 2019; Published 9 April 2019

Academic Editor: Annan Zhou

The dynamic stress-strain relationship of artificial frozen silty clay under one-dimensional coupled static and dynamic loads is obtained using modified split Hopkinson pressure bar (SHPB) equipment. The variation in dynamic compressive strength, dynamic deformation modulus, energy dissipation, and failure mode of artificial frozen silty clay with axial precompressive stress ratio are studied in this research. Experimental results indicate that the dynamic stress-strain curves under uniaxial state and one-dimensional coupled static and dynamic loads can be divided into four stages, i.e., compaction stage, elastic stage, plastic stage, and failure stage. The dynamic compressive strength, first-stage deformation modulus, second-stage deformation modulus, and absorbed energy density of artificial frozen silty clay present a trend of first increase and then decrease with the increase of axial compressive stress ratio, and the axial compressive stress ratio corresponding to the peak value is 0.7 in this test. In addition, there is a very similar effect of axial precompressive stress ratio on dynamic compressive strength and second-stage deformation modulus of artificial frozen silty clay. At 0.4 axial compressive stress ratio, spall phenomenon appears at circumferential direction and center position of the frozen soil specimen has no obvious failure. Shear failure appears at 0.7 to 0.9 axial compressive stress ratio, and the larger the axial compressive stress ratio applies, the more obvious the shearing surface appears; moreover, comminution failure mode appears at 1.0 axial compressive stress ratio.

1. Introduction

The dynamic mechanical property is one of the most important branches of mechanical property of frozen soil, which has attracted extensive attention by scholars in recent years [1–3]. Many studies are conducted to investigate the dynamic mechanical and deformation characteristics of frozen soil using the split Hopkinson pressure bar (SHPB) equipment. The early research primarily concentrates on the dynamic mechanical properties of frozen soil under uniaxial loading state. Moreover, effects of freezing temperature, water content, and strain rate on dynamic stress-strain relationships, strength characteristic, and failure modes are studied experimentally and numerically [4–8]. Previous studies indicate that the dynamic compressive strength of frozen soil increases with the increase of strain rate and the decrease of freezing temperature [4–6]. In addition, studies show that stress state has significant effect on dynamic mechanical property of frozen soil [7, 8].

Artificial freezing method is an environmentally friendly technique to provide temporary excavation support and groundwater control during structural construction, such as shaft and tunnel excavation, metro construction, under difficult geological and hydrological ground conditions [9, 10]. In fact, artificial frozen soils at this condition are subjected to static stresses arising from geostatic stress and frozen-heave force coupled with dynamic loading induced by blasting and machine impact [11, 12]. The mechanical

behaviors of artificial frozen soil under coupled loads are obviously different compared with those under uniaxial loading state. However, not much previous investigations focusing on dynamic mechanical property of frozen soil under different stress states were found. Ma et al. [13] conducted a series of SHPB tests under active confining pressure state for artificial frozen clay and frozen sandy soil, and the effects of active confining pressure on dynamic mechanical property of frozen soil are analyzed. Furthermore, the dynamic constitutive model of frozen soil under active confining pressure are also proposed and verified. Investigations of dynamic behaviors of materials under coupled static and dynamic loads are primary on rock [14–17]. Gong et al. [18] studied the effects of high strain rates and low confining pressures on the dynamic mechanical properties and failure modes of sandstone with a modified triaxial SHPB system. Moreover, the unified dynamic Mohr–Coulomb and Hoek–Brown strength criteria were established based on the obtained test results [19].

However, by summarizing previous theoretical and experimental study achievements, it can be found that researches on the mechanical properties of frozen soil under coupled static and dynamic loads have not been studied. In this paper, the dynamic mechanical and deformation characteristics of artificial frozen silty clay are investigated using the coupled static and dynamic loading test system. In addition, the dynamic stress-strain curve characteristics, dynamic compressive strength, deformation modulus, failure mode, and energy dissipation of artificial frozen silty clay under different axial compressive stress ratios are studied. The results are of certain significance for both studying the property and energy dissipation characteristics of frozen soil and guiding the frozen soil crushing engineering.

2. Experiments and Data Processing

2.1. Artificial Frozen Soil Specimen Preparation. The test frozen silty clay collected from a coalmine in Shanxi Province, China. Detailed explanations and demonstrations on the treating processes of undisturbed soil have been introduced [13]. The property and particle size distribution of silty clay are shown in Tables 1 and 2, respectively. Specimen sizes for static and dynamic tests are $\Phi 50 \times 100$ mm and $\Phi 50 \times 25$ mm, respectively, as shown in Figure 1.

2.2. Coupled Static and Dynamic Loads Tests. Studies [20] have shown that frozen soil in artificial freezing engineering is subjected to confined vertical and horizontal static stresses. In this research, when the frozen soil specimen is subjected to static stress arising from circumferential stress coupled with axial dynamic loading, it is defined as the active confining pressure state. As a contrast, when the specimen is subjected to static stress arising from axial precompressive stress coupled with axial dynamic loading, it is defined as the one-dimensional coupled static and dynamic loads state. The stress schematic of active confining pressure state and one-dimensional coupled static and dynamic loads is shown in Figure 2. SHPB equipment has been successfully used to investigate the dynamic behaviors of materials, such as rock [21], frozen soil, and concrete. In this test, a modified dynamic testing equipment is adopted [18, 19], as shown in Figure 3. It contains a launch device, a spindle-shaped striker, which has benefit of stress balance of frozen soil specimen, an incident bar, a transmitted bar, an axial precompressive stress system, and a buffer bar. The length of incident bar, transmitted bar, and buffer bar are 2000 mm, 1500 mm, and 500 mm, respectively, and the diameters of them are 50 mm. The test procedure is as follows: (1) put artificial frozen soil specimen between the incident bar and transmitted bar; (2) apply axial precompressive stress to the test specimen; (3) close the oil pipe when the value of axial precompressive stress reaches the predetermined value; (4) open launch device and make the striker impact the incident bar.

According to the collected data, the dynamic stress, strain, and strain rate can be calculated through simplified three-wave analysis [22]. In the process of applying axial precompressive stress, a certain amount of elastic strain energy has been deposited inside the frozen soil specimen [23], which can be calculated through

$$E_S = V_S w_S, \tag{1}$$

where E_S is the elastic strain energy deposited inside the specimen, w_S is the elastic strain energy density, and V_S is the volume of specimen. w_S can be calculated through

$$w_S = \int_0^{\varepsilon} \sigma(t) d\varepsilon(t). \tag{2}$$

Thus, the absorbed energy of artificial frozen soil (W_S) can be calculated through the following equation:

$$\begin{aligned} W_S(t) &= E_S + \{W_I(t) - [W_R(t) + W_T(t)]\} \\ &= V_S \int_0^{\varepsilon} \sigma(t) d\varepsilon(t) - \frac{A_0 C_0}{E_0} \int 2\sigma_T \sigma_R dt, \end{aligned} \tag{3}$$

where W_I, W_R, and W_T are the incident energy, reflected energy, and transmitted energy, respectively; E_0, A_0, and C_0 are Young's modulus, the cross-sectional area, and the elastic wave speed of the bar, respectively; σ_T and σ_R are the transmitted stress and reflected stress, respectively; and t is the duration time of elastic wave.

In addition, the concept of absorbed energy density (W) is adopted and defined as the ratio between the absorbed energy and the volume of specimen, which can be described by

$$W = \frac{W_S}{V_S} \times 100\%. \tag{4}$$

2.3. SHPB Tests Design. To investigate the effect of axial precompressive stress on dynamic strength and deformation characteristics of artificial frozen silty clay, the axial precompressive stress ratio (λ) is adopted and defined as the ratio between the axial precompressive stress (σ_{ac}) and the static compressive strength of artificial frozen silty clay (f_c),

Table 1: Property of silty clay.

Soil type	Sample depth (m)	Liquid limit	Plastic limit	Water content	Dry density (g/cm^3)
Silty clay	−383.2~−386.6	28.3%	14.2%	20.06%	2.08

Table 2: Particle size distribution of silty clay.

0~0.075 mm	0.075~0.250 mm	0.250~0.500 mm	0.500~1.000 mm	1.000~2.000 mm
10.50%	49.54%	14.37%	21.71%	3.88%

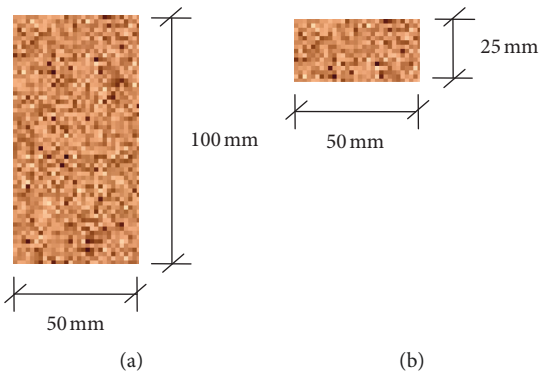

Figure 1: Artificial frozen silty clay specimens for static and dynamic tests. (a) Static test specimen. (b) Dynamic test specimen.

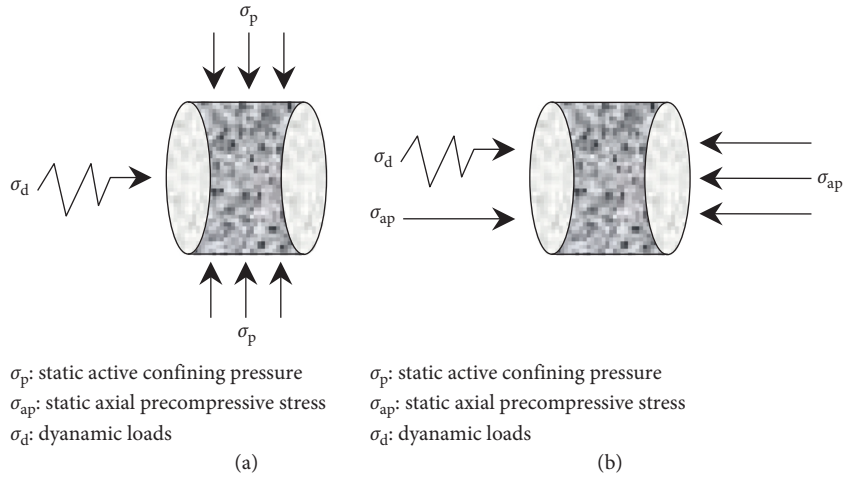

Figure 2: Schematic of frozen soil under different stress states. (a) Active confining pressure state. (b) One-dimensional coupled static and dynamic loads.

as shown in equation (5). In contrast, the static compressive tests of artificial frozen silty clay are also conducted. The SHPB tests design is shown in Table 3:

$$\lambda = \frac{\sigma_{ac}}{f_c}. \quad (5)$$

3. Test Results

3.1. Static Test Results. To ensure the reliability of test results, three artificial frozen soil specimens are prepared and tested for each case and the average value of experimental data are recorded. The static stress-strain curves are shown in Figure 4. It is obvious that the static stress-strain curve of artificial frozen silty clay at −10°C can be divided into three stages, i.e., elastic stage, plastic stage, and failure stage. The average static compressive strength is 2.73 MPa. Figure 5 demonstrates that shear failure appears in the static test.

3.2. Coupled Static and Dynamic Loads Tests Results. In the present study, the purpose of SHPB tests on the artificial frozen silty clay specimen is to obtain the dynamic stress-strain relationships and study the effects of axial pre-compressive stress ratio on dynamic performance (e.g., dynamic compressive strength, deformation modulus, failure mode, and energy dissipation). Results obtained from

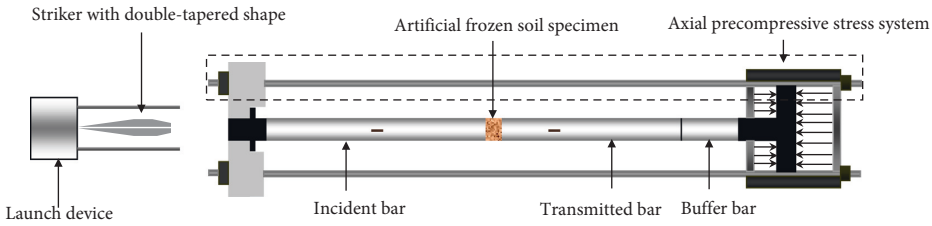

Figure 3: Modified SHPB equipment [18, 19].

Table 3: SHPB test design of artificial frozen silty clay.

Soil type	Freezing temperature (°C)	Strain rate (s^{-1})	λ
Silty clay	−10	364~399	0.3, 0.4, 0.5, 0.6, 0.7, 0.8, 0.9, 1.0

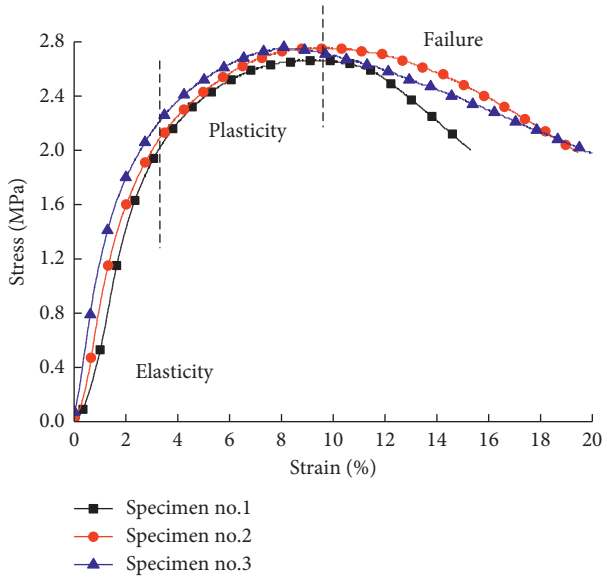

Figure 4: Static stress-strain curves of artificial frozen silty clay at −10°C.

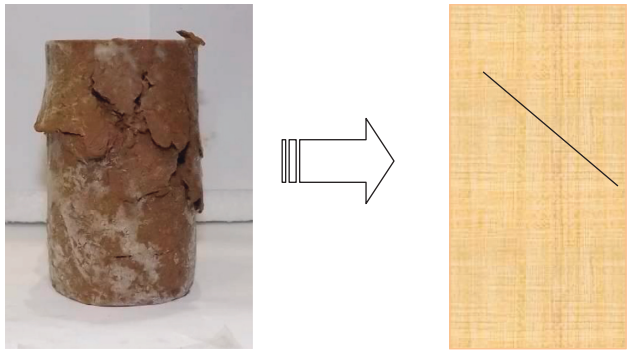

Figure 5: Failure mode of artificial frozen silty clay at −10°C.

dynamic impact tests are summarized in the following sections.

3.2.1. Dynamic Stress-Strain Curves. Figure 6 shows the representative dynamic stress-strain curves of artificial frozen silty clay under uniaxial state and one-dimensional

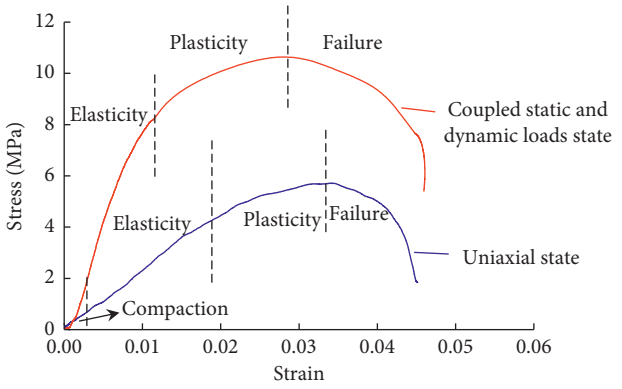

Figure 6: Dynamic stress-strain curves of artificial frozen silty clay at −10°C.

coupled static and dynamic loads. It can be concluded that dynamic stress-strain curves can be divided into four stages, i.e., compaction stage, elastic stage, plastic stage, and failure stage under two states. Additionally, the compaction stage of the curve under one-dimensional coupled static and dynamic loads state is less obvious compared with that under uniaxial state.

3.2.2. Dynamic Compressive Strength and Deformation Modulus. In this test, dynamic compressive strength (σ_d) is defined as the dynamic peak stress in dynamic stress-strain curves. The defining method of deformation modulus is as follows: (1) the first-stage deformation modulus (E_1) is defined as the slope of the line from the origin to the point at which the stress is 50% peak stress on the stress-strain curve; (2) the second-stage deformation modulus (E_2) is defined as the slope of line from the point of 50% peak stress to the point corresponding to peak stress on the stress-strain curve [24], as shown in Figure 7.

According to the defining methods of strength and deformation modulus, the experimental results of artificial frozen silty clay under different axial precompressive stress ratios are shown in Figures 8–10. The figures reveal that (1) dynamic compressive strength, first-stage deformation modulus, and second-stage deformation modulus of

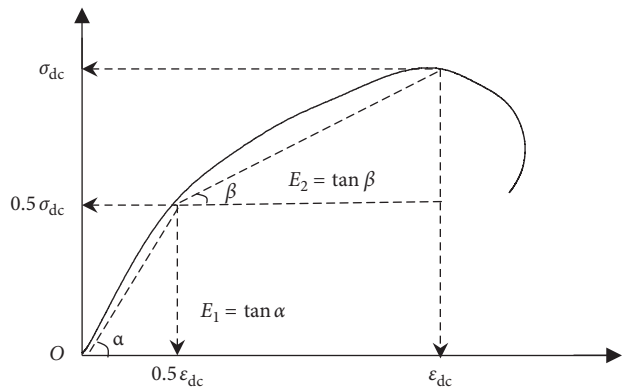

Figure 7: Defining methods of deformation modulus under one-dimensional coupled static and dynamic loads [24].

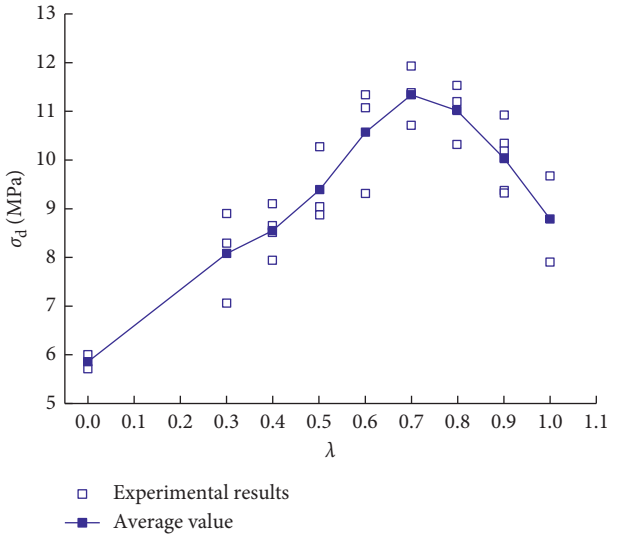

Figure 8: Variation in dynamic compressive strength of artificial frozen silty clay with axial precompressive stress ratio.

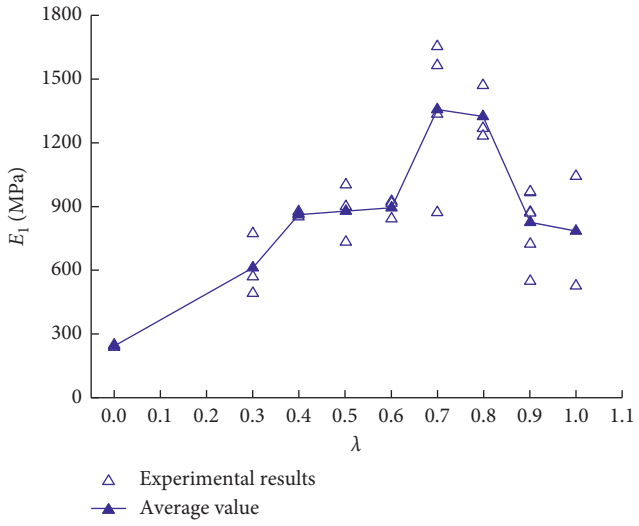

Figure 9: Variation in first-stage deformation modulus of artificial frozen silty clay with axial precompressive stress ratio.

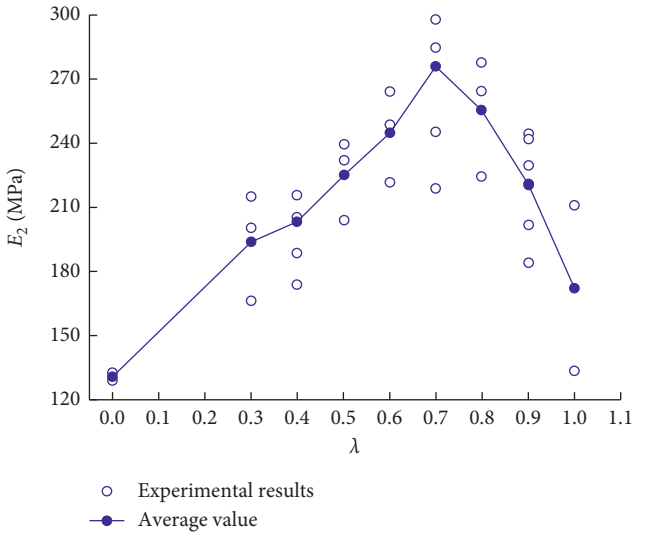

Figure 10: Variation in second-stage deformation modulus of artificial frozen silty clay with axial precompressive stress ratio.

artificial frozen silty clay under one-dimensional coupled loads are higher than those under uniaxial state. For example, the average values of σ_d, E_1, and E_2 at 0.3 axial precompressive stress ratio are 8.08 MPa, 611.42 MPa, and 193.88 MPa, respectively, which are higher than the value of 5.86 MPa, 243.28 MPa, and 130.78 MPa under uniaxial state; (2) σ_d, E_1, and E_2 present a trend of first increase and then decrease with the increase of axial compressive stress ratio, and the axial compressive stress ratio corresponding to their peak values is 0.7. Their average values at 0.7 axial precompressive stress ratio are 11.34 MPa, 1356.25 MPa, and 275.89 MPa, respectively, which is 1.94, 5.57, and 2.11 times higher than those under uniaxial state. The results indicate that the effect of axial compressive stress ratio on E_1 is larger than that on σ_d and E_2.

The mechanism behind this phenomenon can be clarified as follows: (1) If the axial precompressive stress ratio is less than 0.7, from the static stress-strain curves of artificial frozen silty clay, it can be noticed that the frozen soil specimen remains in the elasticity stage and microcracks and voids inside the frozen soil specimen will be closed. Therefore, more stress waves will propagate through the specimen, resulting in the increase of dynamic mechanical parameters. (2) If the axial precompressive stress ratio exceeds 0.7, it is obvious that the internal microdamages and macrodamages will generate and develop inside frozen soil specimen, resulting in the degradation of frozen soil specimen. In this case, more stress wave will be reflected, resulting in the decrease of dynamic mechanical parameters.

Based on the above analysis, we can conclude that σ_d, E_1, and E_2 present a similar trend of first increase and then decrease with the increase of axial precompressive stress ratio. To investigate the internal relationships between the above three important parameters and axial precompressive stress ratio, the strength growth factor (σ_{dcf}), first-stage deformation modulus growth factor (E_{1f}), and second-stage deformation modulus growth factor (E_{2f}) are

adopted to demonstrate change rules. The definition of σ_{dcf}, E_{1f}, and E_{2f} can be described by

$$\sigma_{dcf} = \frac{\sigma_{dc\lambda}}{\sigma_{dc0}},$$
$$E_{1f} = \frac{E_{1\lambda}}{E_{10}}, \quad (6)$$
$$E_{2f} = \frac{E_{2\lambda}}{E_{20}},$$

where $\sigma_{dc\lambda}$, $E_{1\lambda}$, and $E_{2\lambda}$ are the dynamic compressive strength, the first-stage deformation modulus, the second-stage deformation modulus of artificial frozen silty clay with different axial precompressive stress ratios, respectively; σ_{dc0}, E_{10}, and E_{20} are the dynamic compressive strength, the first-stage deformation modulus, the second-stage deformation modulus of artificial frozen silty clay under uniaxial state, respectively.

According to the calculation methods, the σ_{dcf}, E_{1f}, and E_{2f} with different axial precompressive stress ratios are calculated and illustrated in Figure 11. Figure 11 reveals that there is a very similar effect of axial precompressive stress ratio on σ_{dcf} and E_{2f}. However, the variation trend of E_{1f} is clearly different from that of σ_{dcf} and E_{2f}. The $E_{1\lambda}$ reflects the deformation capability of artificial frozen silty clay at the elastic stage; however, $E_{2\lambda}$ reflects the deformation capability at the plastic stage, which corresponds to the damage evolution process of the specimen, and many studies results have testified that the materials strength is effected by the damage evolution process [25–27]. Therefore, similar variation trend can be found about σ_{dcf} and E_{2f}.

3.2.3. Dynamic Failure Mode. In frozen soil crushing engineering, studying the failure mode of artificial frozen soil has important significance for improving the crushing efficiency. The failure modes of artificial frozen silty clay under different axial compressive stress ratios are shown in Figure 12.

Figure 12 reveals that the axial compressive stress ratio has significant effect on the failure mode of artificial frozen silty clay. Three typical failure modes are found under one-dimensional coupled static and dynamic loads, as described in the following: (1) At 0.4 axial compressive stress ratio, spall phenomenon appears in circumferential direction and center position of the frozen soil specimen has no obvious failure. (2) Shear failure appears at 0.7 to 0.9 axial compressive stress ratio, and the larger the axial compressive stress ratio, the more obvious the shearing surface appears, and moreover, the comminuted area close to the incident bar is greater than that close to the reflected bar, which is caused by the attenuation of stress waves [28]. (3) Comminution mode appears at 1.0 axial compressive stress ratio.

3.2.4. Dynamic Energy Dissipation. Absorbed energy density (W) is one of the most important parameters in frozen soil crushing engineering [29]. The absorbed energy density under different axial compressive stress ratios are calculated based on equation (4), as shown in Figure 13. With the

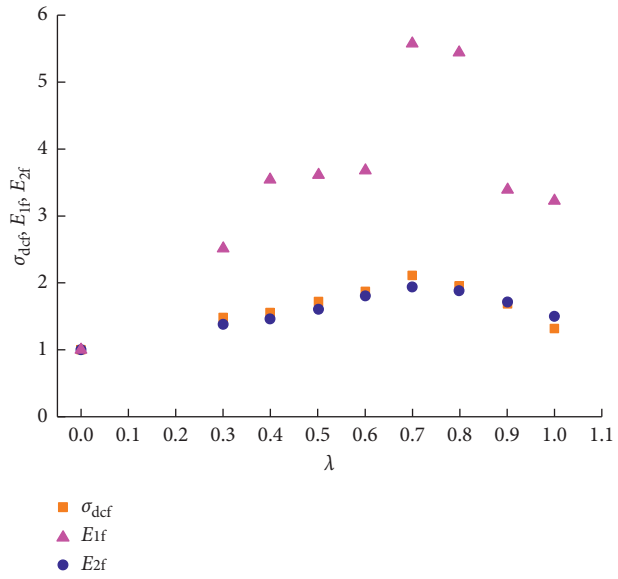

Figure 11: σ_{dcf}, E_{1f}, and E_{2f} of artificial frozen silty clay with different axial compressive stress ratios.

increase of axial compressive stress ratio, the absorbed energy density first increase and then decrease. The average absorbed energy density increases from 0.179 J/cm^3 to 0.417 J/cm^3 when the axial compressive stress ratio increases from 0 to 0.7. In other words, the absorbed energy of frozen soil specimen under 0.7 axial compressive stress ratio is 2.33 times larger than that under uniaxial state. However, when the axial compressive stress ratio reaches 1.0, average absorbed energy density decreases to 0.266 J/cm^3, which shows 36.21% lower than that under 0.7 axial compressive stress ratio. The results indicate that change in the axial compressive stress of frozen soil appropriately can improve the crushing efficiency and reduce the energy consumption. This finding is of great value to design the crushing parameters in frozen soil crushing engineering. This phenomenon demonstrates that, in this research, the capacity of frozen soil specimen resistance is the biggest at about 0.7 axial compressive stress ratio, leading to absorb more energy to reach the failure state.

4. Conclusions

The dynamic mechanical properties of artificial frozen silty clay are tested using modified SHPB equipment, and the effects of axial compressive stress ratio on dynamic stress-strain curves, dynamic compressive strength, deformation modulus, energy dissipation, and failure mode of artificial frozen silty clay are investigated in this research. The main conclusions are as follows:

(1) The dynamic stress-strain curves under uniaxial state and one-dimensional coupled static and dynamic loads can be divided into four stages, i.e., compaction stage, elastic stage, plastic stage, and failure stage, and the compaction stage of the curve under coupled loads is not obvious compared with that under uniaxial state.

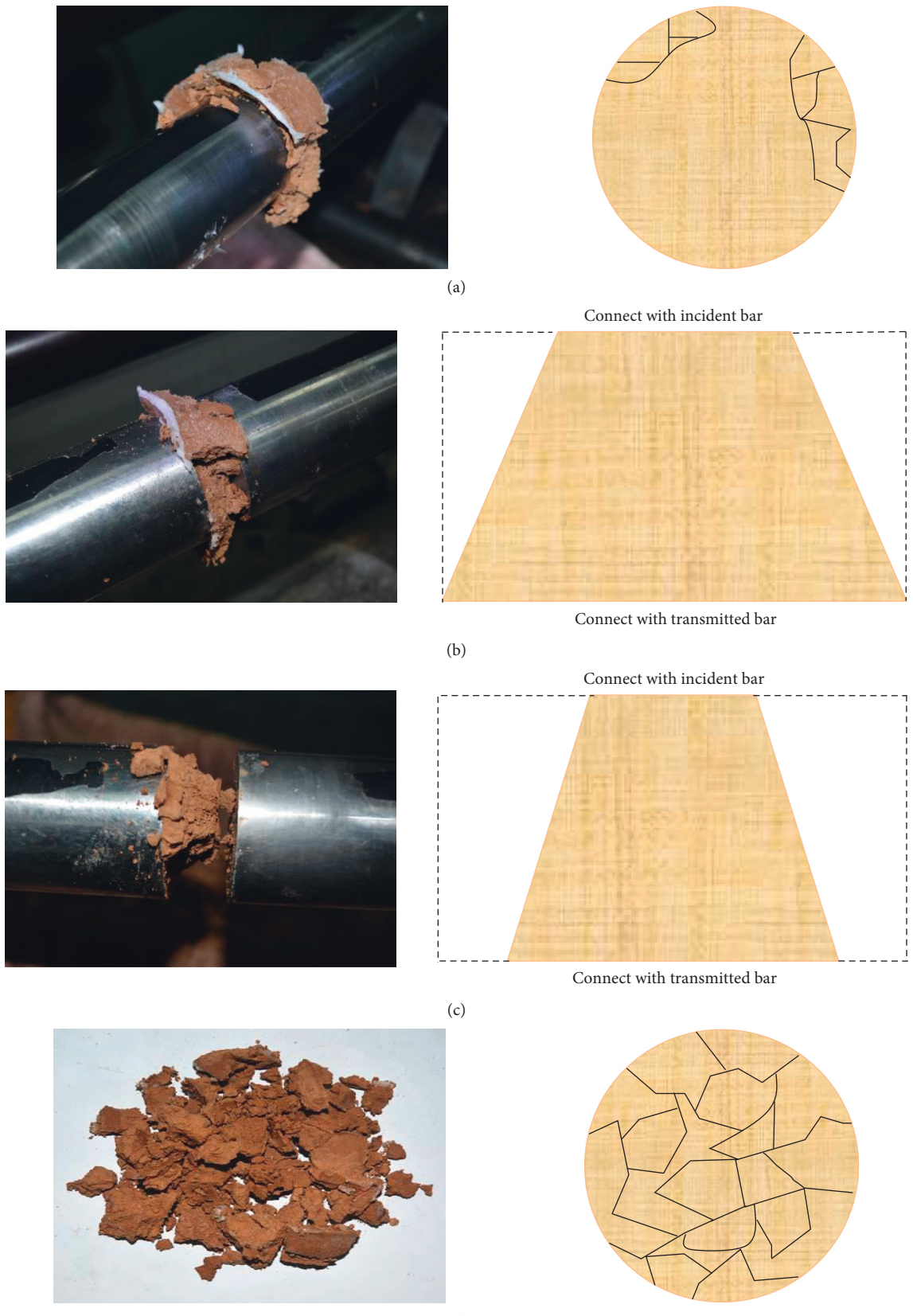

Figure 12: Failure modes of artificial frozen silty clay with different axial compressive stress ratios under one-dimensional coupled static and dynamic loads. (a) Failure mode of artificial frozen silty clay with 0.4 λ. (b) Failure mode of artificial frozen silty clay with 0.7 λ. (c) Failure mode of artificial frozen silty clay with 0.9 λ. (d) Failure mode of artificial frozen silty clay with 1.0 λ.

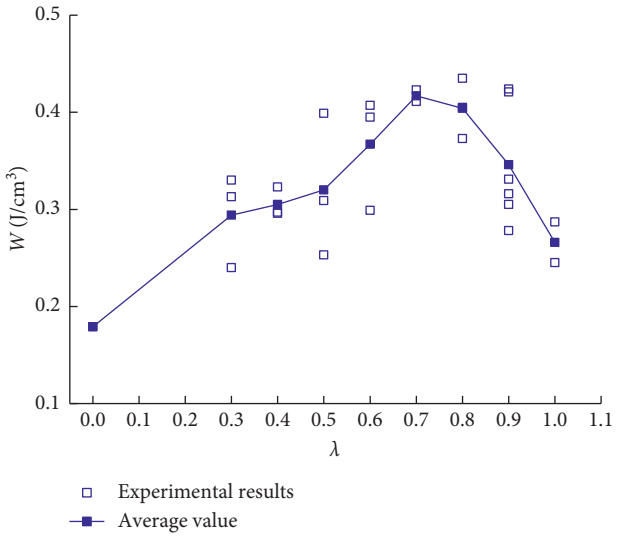

Figure 13: Dissipated energy density of artificial frozen silty clay with different axial compressive stress ratios under coupled loads.

(2) With the increase of axial compressive stress ratio, the dynamic compressive strength, first-stage deformation modulus, second-stage deformation modulus, and absorbed energy density of artificial frozen silty clay under one-dimensional coupled loads are higher than those under uniaxial state. Both of them present a trend of first increase and then decrease with the increase of axial compressive stress ratio, and the axial compressive stress ratio corresponding to their peak values is 0.7 in this test. In addition, there is a very similar effect of axial precompressive stress ratio on dynamic compressive strength and second-stage deformation modulus of artificial frozen silty clay.

(3) Three typical failure modes are found under one-dimensional coupled static and dynamic loads. At 0.4 axial compressive stress ratio, spall phenomenon appears at circumferential direction and center position of frozen soil specimen has no obvious failure. Shear failure appears at 0.7 to 0.9 axial compressive stress ratio, and the larger the axial compressive stress ratio applies, the obvious the shearing surface appears; moreover, the comminuted area close to the incident bar is greater than that close to the reflected bar. Comminution mode appears at 1.0 axial compressive stress ratio.

Data Availability

The datasets generated and analyzed during the current study are available from the corresponding author on reasonable request.

Conflicts of Interest

The authors declare that there are no conflicts of interest regarding the publication of this paper.

Acknowledgments

This research received financial support from Anhui Provincial Natural Science Foundation (No. 1908085QE212) and Postgraduate Innovation Fund Project in Anhui University of Science & Technology (No. 2017CX1001). The authors thank the Engineering Research Center of Underground Mine Construction, Ministry of Education, and Anhui University of Science & Technology for providing the experiment conditions.

References

[1] Q. Y. Ma, *Frozen Soil Blasting and Drilling Test and Its Application*, Science Press, Beijing, China, 2007.

[2] Q. Y. Ma, "Research status of dynamic properties of artificial frozen soil and its significance," *Rock and Soil Mechanics*, vol. 30, no. 1, pp. 10–14, 2009.

[3] Q. Xie, Z. Zhu, and G. Kang, "Dynamic stress-strain behavior of frozen soil: experiments and modeling," *Cold Regions Science and Technology*, vol. 106-107, pp. 153–160, 2014.

[4] Q. Xie, Z. Zhu, and G. Kang, "A dynamic micromechanical constitutive model for frozen soil under impact loading," *Acta Mechanica Solida Sinica*, vol. 29, no. 1, pp. 13–21, 2016.

[5] Q.-Y. Ma, "Experimental analysis of dynamic mechanical properties for artificially frozen clay by the split Hopkinson pressure bar," *Journal of Applied Mechanics and Technical Physics*, vol. 51, no. 3, pp. 448–452, 2010.

[6] Z. Zhu, G. Kang, Y. Ma, Q. Xie, D. Zhang, and J. Ning, "Temperature damage and constitutive model of frozen soil under dynamic loading," *Mechanics of Materials*, vol. 102, pp. 108–116, 2016.

[7] H.-D. Zhang, Z.-W. Zhu, S.-C. Song, G.-Z. Kang, and J.-G. Ning, "Dynamic behavior of frozen soil under uniaxial strain and stress conditions," *Applied Mathematics and Mechanics*, vol. 34, no. 2, pp. 229–238, 2013.

[8] Q. Y. Ma, J. S. Zhang, W. F. Chen, and P. Yuan, "Analysis of SHPB test and impact compression in confining pressure for artificial frozen soil," *Rock and Soil Mechanics*, vol. 35, no. 3, pp. 637–640, 2014.

[9] A. Marwan, M.-M. Zhou, M. Zaki Abdelrehim, and G. Meschke, "Optimization of artificial ground freezing in tunneling in the presence of seepage flow," *Computers and Geotechnics*, vol. 75, pp. 112–125, 2016.

[10] D.-J. Zhao, Y.-M. Liu, Y.-H. Sun, Y. Zhao, and F.-T. Bai, "Experiments and simulations of underground artificial freezing with the use of natural cold resources in cold regions," *Building and Environment*, vol. 87, pp. 224–233, 2015.

[11] D. D. Ma, Q. Y. Ma, P. Yuan, and Z. M. Yao, "SHPB tests on artificial frozen sand and its analysis under active confining pressure," *Rock and Soil Mechanics*, vol. 38, no. 10, pp. 2957–2961, 2017.

[12] D. D. Ma, Q. Y. Ma, P. Yuan, and Z. M. Yao, "Comparison analysis and SHPB tests on artificial frozen clay in uniaxial load and confining pressure states," *Journal of Vibration and Shock*, vol. 36, no. 19, pp. 255–260, 2017.

[13] D. Ma, Q. Ma, and P. Yuan, "SHPB tests and dynamic constitutive model of artificial frozen sandy clay under confining pressure and temperature State," *Cold Regions Science and Technology*, vol. 136, pp. 37–43, 2017.

[14] X. Li, F. Gong, M. Tao et al., "Failure mechanism and coupled static-dynamic loading theory in deep hard rock mining: a

review," *Journal of Rock Mechanics and Geotechnical Engineering*, vol. 9, no. 4, pp. 767–782, 2017.

[15] X. Li, M. Tao, C. Wu, K. Du, and Q. Wu, "Spalling strength of rock under different static pre-confining pressures," *International Journal of Impact Engineering*, vol. 99, pp. 69–74, 2017.

[16] M. Tao, A. Ma, W. Cao, X. Li, and F. Gong, "Dynamic response of pre-stressed rock with a circular cavity subject to transient loading," *International Journal of Rock Mechanics and Mining Sciences*, vol. 99, pp. 1–8, 2017.

[17] F. Q. Gong and G. F. Zhao, "Dynamic Indirect tensile strength of sandstone under different loading rates," *Rock Mechanics and Rock Engineering*, vol. 47, no. 6, pp. 2271–2278, 2014.

[18] F.-Q. Gong, X.-F. Si, X.-B. Li, and S.-Y. Wang, "Dynamic triaxial compression tests on sandstone at high strain rates and low confining pressures with split Hopkinson pressure bar," *International Journal of Rock Mechanics and Mining Sciences*, vol. 113, pp. 211–219, 2019.

[19] X. Si, F. Gong, X. Li, S. Wang, and S. Luo, "Dynamic Mohr-Coulomb and Hoek-Brown strength criteria of sandstone at high strain rates," *International Journal of Rock Mechanics and Mining Sciences*, vol. 115, pp. 48–59, 2019.

[20] X. Li, Z. Zhou, T.-S. Lok, L. Hong, and T. Yin, "Innovative testing technique of rock subjected to coupled static and dynamic loads," *International Journal of Rock Mechanics and Mining Sciences*, vol. 45, no. 5, pp. 739–748, 2008.

[21] M. Li, X. Mao, H. Pu, Y. Chen, Y. Wu, and L. Zhang, "Effects of heating rate on the dynamic tensile mechanical properties of coal sandstone during thermal treatment," *Shock and Vibration*, vol. 2017, Article ID 2619081, 12 pages, 2017.

[22] P. Yuan and Y. Xu, "Influence of curing time on impact energy absorption characteristics of artificially cemented sand," *Journal of Vibroengineering*, vol. 19, no. 6, pp. 4033–4041, 2017.

[23] F. Q. Gong, X. B. Li, and X. L. Liu, "Preliminary experimental study of characteristics of rock subjected to 3D coupled static and dynamic loads," *Chinese Journal of Rock Mechanics and Engineering*, vol. 30, no. 6, pp. 1179–1190, 2011.

[24] F. Q. Gong, X. B. Li, X. L. Liu, and J. Zhao, "Experimental study of dynamic characteristic of sandstone under one-dimensional coupled static and dynamic loads," *Chinese Journal of Rock Mechanics and Engineering*, vol. 29, no. 10, pp. 2076–2085, 2010.

[25] E. Quirino, S. Dariusz, S. A. Jesus, M. Tadeusz, V. V. Julio, and R. M. Alejandro, "Crashworthiness behavior of aluminum profiles with holes considering damage criteria and damage evolution," *International Journal of Mechanical Sciences*, vol. 131-132, pp. 776–791, 2017.

[26] H. Li, H. Yang, R. D. Lu, and M. W. Fu, "Coupled modeling of anisotropy variation and damage evolution for high strength steel tubular materials," *International Journal of Mechanical Sciences*, vol. 105, pp. 41–57, 2016.

[27] W. Zhu, L. Liu, J. Liu, C. Wei, and Y. Peng, "Impact of gas adsorption-induced coal damage on the evolution of coal permeability," *International Journal of Rock Mechanics and Mining Sciences*, vol. 101, pp. 89–97, 2018.

[28] L. L. Wang, *Foundation of Stress Waves*, Elsevier, Amsterdam, Netherlands, 2007.

[29] Q. Y. Ma, D. D. Ma, P. Yuan, and Z. M. Yao, "Energy absorption characteristics of frozen soil based on SHPB test," *Advances in Materials Science and Engineering*, vol. 2018, Article ID 5378173, 9 pages, 2018.